# Chapter 10

# Dipole emission near planar interfaces

The problem of dipole radiation in or near planarly layered media is of significance to many fields of study. It is encountered in antenna theory, single molecule spectroscopy, cavity quantum electrodynamics, integrated optics, circuit design (microstrips), and surface contamination control. The theory was also applied to explain the strongly

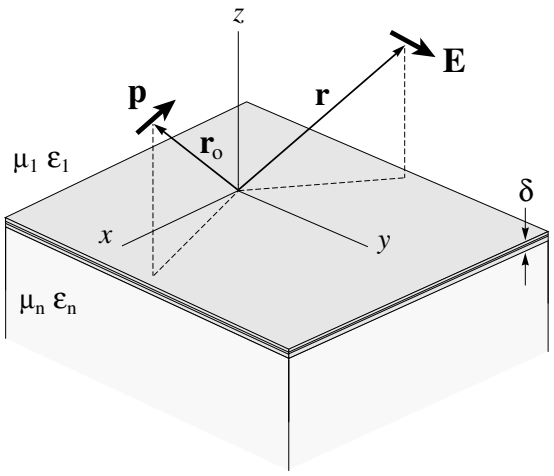


Figure 10.1: Configuration of the dipole problem. The dipole is located at $\mathbf{r}_o = (x_o, y_o, z_o)$ and the planar interfaces are characterized by $z = const.$. The surface of the topmost layer coincides with the coordinate origin. The properties of the upper and lower half-spaces are designated by the index 1 and $n$, respectively.

enhanced Raman effect of adsorbed molecules on noble metal surfaces, and in surface science and electrochemistry for the study of optical properties of molecular systems adsorbed on solid surfaces. Detailed literature on the latter topic is given in Ref. [1]. In the context of near-field optics, dipoles close to a planar interface have been considered by various authors to simulate tiny light sources and small scattering particles [2]. The acoustic analogue is also applied to a number of problems such as seismic investigations or ultrasonic detection of defects in materials [3].

In his original paper [4], in 1909, Sommerfeld developed a theory for a radiating dipole oriented vertically above a planar and lossy ground. He found two different asymptotic solutions: space waves (spherical waves) and surface waves. The latter had already been investigated by Zenneck [5]. Sommerfeld concluded that surface waves account for long-distance radio wave transmission because of their slower radial decay along the Earth's surface compared with space-waves. Later, when space waves were found to reflect at the ionosphere, the contrary was confirmed. Nevertheless, Sommerfeld's theory formed the basis for all subsequent investigations. In 1911 Hörschelmann [6, 7], a student of Sommerfeld, analyzed the horizontal dipole in his doctoral dissertation and used likewise expansions in cylindrical coordinates. Later, in 1919, Weyl [8] expanded the problem by a superposition of plane and evanescent waves (angular spectrum representation), and similar approaches were developed by Strutt [9], Van der Pol and Niessen [10]. Agarwal later used the Weyl representation to extend the theory to quantum electrodynamics [11]. Due to the overwhelming amount of literature many aspects of the theory were reinvented over the years, probably caused by the fact that the early literature was written in German. An English version of the early developments is summarized in Sommerfeld's lectures on theoretical physics [12].

At first glance, the calculation of the field of a dipole near planar interfaces seems to be an easy task. The primary dipole field (free space Green's function) possesses a simple mathematical description, and the planar interfaces have reduced dimensionality. Furthermore, the planar interfaces are constant coordinate surfaces for different coordinate systems. It is therefore very astonishing that there is no closed solution for this elementary problem, not even for the vertically oriented dipole which has a perfect rotational symmetry. The desired simplicity is only obtained for limiting cases, such as ideally conducting interfaces or the quasi-static limit.

### 10.0.1 Allowed and forbidden light

Let us consider the situation shown in Fig. 10.1 where a dipole is located above a layered substrate. We assume that the lower half-space (substrate) is optically denser than the upper half-space (vacuum). If the distance of the dipole from the surface of the layer is less than one wavelength, *evanescent* field components of the dipole

interact with the layered structure and excite thereby other forms of electromagnetic radiation. Their energy can either be (1) absorbed by the layer, (2) transformed into propagating waves in the lower half space, or (3) coupled to modes propagating along the layer. In the second case the plane waves propagate in directions beyond the critical angle of total internal reflection $\alpha_c = \arcsin(n_1/n_3)$, where $n_1$ and $n_3$ are the refraction coefficients of the upper and lower half space, respectively. The amplitude of the plane waves depends exponentially on the height of the dipole above the layer. Thus, for dipoles separated more than a couple of wavelengths from the surface there will be virtually no light coupled into directions beyond the critical angle. This is why the light at supercritical angles is denoted as *forbidden light* [13].

Fig. 10.2 illustrates the difference between allowed and forbidden light. Here, we assume that $\varepsilon_3 > \varepsilon_1 > \varepsilon_2$. In configuration ($a$) a dielectric interface is illuminated by a plane wave incident from the upper medium in such a way that a propagating transmitted wave exists. If a second interface is brought close, the light transmitted into the downmost medium does not depend, apart from interference undulations, on the spacing between the two interfaces and the transmitted light propagates into a direction which is within the critical angle of total internal reflection. The situation in ($b$) is quite different from the previous one. Here, the wave hits the upper interface in such a way that no transmitted field exists. Instead, an evanescent wave is formed,

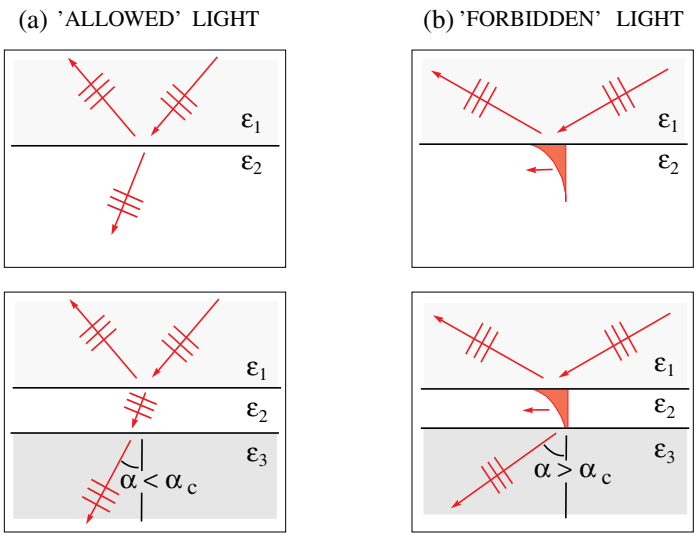


Figure 10.2: Illustration of allowed and forbidden light. The three media fulfill $\varepsilon_3 > \varepsilon_1 > \varepsilon_2$. The incident wave hits the upper interface in such a way that (a) a transmitted wave exists and (b) the wave is totally reflected.

decaying exponentially in normal direction and propagating along the interface. If the second interface is approached, the evanescent wave will be transformed into a propagating wave in the lowest region (optical tunneling). This wave propagates in directions beyond the critical angle of total internal reflection and depends sensitively on the gap between the two interfaces.

## 10.1 Angular spectrum representation of the dyadic Green's function

The solution to the problem depicted in Fig. 10.1 has to be expanded by suitable functions satisfying Maxwell's equations. In order to fulfill the boundary conditions analytically, the functions have to be orthogonal on the interfaces. This is true for expansions in both Cartesian and cylindrical coordinates. Both treatments have their advantages and disadvantages and lead to integrals which cannot be solved analytically. Sommerfeld used expansions in cylindrical waves. This approach is very efficient from a computational point of view since the fields are represented by only one single integral. A detailed account of Sommerfeld's approach can be found in Ref. [2]. Here, we will adopt an expansion in plane and evanescent waves (angular spectrum representation) because the results are physically more intuitive. Furthermore, with suitable substitutions it is straightforward to transform the results at a later stage from a Cartesian system to a cylindrical system. In order to account for all possible orientations of the dipole we will use the dyadic Green's function formalism outlined earlier in Section **??**.

Let us first review the dipole fields in a homogeneous, linear and isotropic medium. In this case, the interfaces in Fig. 10.1 are removed and the entire space is characterized by $\varepsilon_1$ and $\mu_1$. The dyadic Green's function $\overleftrightarrow{\mathbf{G}}_o\,(\mathbf{r},\mathbf{r}_o)$ defines the electric field $\mathbf{E}(\mathbf{r})$ of an electric dipole $\boldsymbol{\mu}$ located at $\mathbf{r}_o=(x_o,y_o,z_o)$ according to

$$\mathbf{E}(\mathbf{r}) \;=\; \omega^2\mu_o\mu_1\,\overleftrightarrow{\mathbf{G}}_o\,(\mathbf{r},\mathbf{r}_o)\,\boldsymbol{\mu}\,. \tag{10.1}$$

The material parameters and the oscillation frequency determine the wavenumber $k_1$ and its longitudinal component $k_{z_1}$. To represent $\overleftrightarrow{\mathbf{G}}_o$ by an angular spectrum we first consider the vector potential $\mathbf{A}$ which satisfies [c.f. Eq. (**??**)]

$$\left[\nabla^2+k_1^2\right]\mathbf{A}(\mathbf{r}) \;=\; -\mu_o\mu_1\,\mathbf{j}(\mathbf{r})\,. \tag{10.2}$$

Here, $\mathbf{j}$ is the current density of the dipole which reads as

$$\mathbf{j}(\mathbf{r}) \;=\; -i\omega\,\delta(\mathbf{r}-\mathbf{r}_o)\;\boldsymbol{\mu}\,. \tag{10.3}$$

Using the definition of the scalar Green's function $G_o$ [c.f. Eq. (**??**)] we obtain

$$\mathbf{A}(\mathbf{r}) \;=\; \boldsymbol{\mu}\,\frac{k_1^2}{i\omega\varepsilon_o\varepsilon_1}\,\frac{\mathrm{e}^{ik_1|\mathbf{r}-\mathbf{r}_o|}}{4\pi|\mathbf{r}-\mathbf{r}_o|}\,. \tag{10.4}$$

where we used Eq. (**??**). Notice, that the vector potential is polarized in direction of the dipole moment. We now introduce the Weyl identity defined in Section **??** and rewrite the vector potential as

$$\mathbf{A}(\mathbf{r}) \;=\; \boldsymbol{\mu}\,\frac{k_1^2}{8\pi^2\omega\varepsilon_o\varepsilon_1}\iint_{-\infty}^{\infty}\frac{1}{k_{z_1}}\,\mathrm{e}^{i\left[k_x(x-x_o)+k_y(y-y_o)+k_{z_1}|z-z_o|\right]}\,dk_x\,dk_y\,. \tag{10.5}$$

Using $\mathbf{E}=i\omega[1+k_1^{-2}\nabla\nabla\cdot]\mathbf{A}$ it is straightforward to derive the electric field. Similarly, the magnetic field is calculated using $\mathbf{H}=(\mu_o\mu_1)^{-1}\nabla\times\mathbf{A}$. The resulting expression for $\mathbf{E}$ can be compared with Eq. (10.1) which allows us to identify the dyadic Green's function as

$$\boxed{\begin{aligned}\overleftrightarrow{\mathbf{G}}_o(\mathbf{r},\mathbf{r}_o) &= \frac{i}{8\pi^2}\iint_{-\infty}^{\infty}\overleftrightarrow{\mathbf{M}}\,\mathrm{e}^{i\left[k_x(x-x_o)+k_y(y-y_o)+k_{z_1}|z-z_o|\right]}\,dk_x\,dk_y\\ \overleftrightarrow{\mathbf{M}} &= \frac{1}{k_1^2k_{z_1}}\begin{bmatrix} k_1^2-k_x^2 & -k_xk_y & \mp k_xk_{z_1}\\ -k_xk_y & k_1^2-k_y^2 & \mp k_yk_{z_1}\\ \mp k_xk_{z_1} & \mp k_yk_{z_1} & k_1^2-k_{z_1}^2\end{bmatrix}\end{aligned}} \tag{10.6}$$

Some terms in the matrix $\overleftrightarrow{\mathbf{M}}$ have two different signs. This originates from the absolute value $|z-z_o|$. The upper sign applies for $z>z_o$ and the lower sign for $z<z_o$. Eq. (10.6) allows us to express the fields of an arbitrarily oriented dipole in terms of plane waves and evanescent waves.

## 10.2 Decomposition of the dyadic Green's function

In order to apply the Fresnel reflection and transmission coefficients to the dipole fields it is necessary to split $\overleftrightarrow{\mathbf{G}}$ into a s-polarized part and a p-polarized part. This decomposition can be accomplished by dividing the matrix $\overleftrightarrow{\mathbf{M}}$ into the two parts

$$\overleftrightarrow{\mathbf{M}}(k_x,k_y) \;=\; \overleftrightarrow{\mathbf{M}}^{s}(k_x,k_y) \;+\; \overleftrightarrow{\mathbf{M}}^{p}(k_x,k_y)\,, \tag{10.7}$$

where we realize that a dipole oriented perpendicular to the planar interfaces in Fig. 10.1 renders a purely p-polarized field. This follows from the fact that the magnetic field of an electric dipole has only a $H_\phi$ component [c.f. Eq. (**??**)] which is

parallel to the interfaces for $\boldsymbol{\mu} = p\,\mathbf{n}_z$. Similarly, a magnetic dipole oriented perpendicular to the interfaces leads to a purely s-polarized field. We therefore define the following potentials*

$$\mathbf{A}^e(\mathbf{r}) \;=\; A^e(\mathbf{r})\;\mathbf{n}_z \tag{10.8}$$

$$\mathbf{A}^h(\mathbf{r}) \;=\; A^h(\mathbf{r})\;\mathbf{n}_z\;, \tag{10.9}$$

and relate them to the electric and magnetic fields as

$$\mathbf{E} \;=\; i\omega[1+\frac{1}{k_1^2}\nabla\nabla\cdot]\,\mathbf{A}^e \;-\; \frac{1}{\varepsilon_o\varepsilon_1}\nabla\times\mathbf{A}^h \tag{10.10}$$

$$\mathbf{H} \;=\; i\omega[1+\frac{1}{k_1^2}\nabla\nabla\cdot]\,\mathbf{A}^h \;+\; \frac{1}{\mu_o\mu_1}\nabla\times\mathbf{A}^e\;. \tag{10.11}$$

Here, $\mathbf{A}^e$ and $\mathbf{A}^h$ render a purley p-polarized field and a purely s-polarized field, respectively. To proceed, we introduce the angular spectrum representation of the potentials $A^e$ and $A^h$ as

$$A^{e,h}(x,y,z) \;=\; \frac{1}{2\pi}\iint_{-\infty}^{\infty}\hat{A}^{e,h}(k_x,k_y)\;\mathrm{e}^{i\left[k_x(x-x_o)+k_y(y-y_o)+k_{z_1}|z-z_o|\right]}\,dk_x\,dk_y\,, \tag{10.12}$$

and introduce it with Eq. (10.8) and Eq. (10.9) into Eq. (10.10). The resulting expression for the electric field can be compared with the field generated by the dyadic Green's function derived in the previous section. This comparison allows us to identify the Fourier spectra $\hat{A}^e$ and $\hat{A}^h$ as

$$\hat{A}^e(k_x,k_y) \;=\; \frac{\omega\mu_o\mu_1}{4\pi}\,\frac{\mp\mu_x\,k_xk_{z_1}\;\mp\;\mu_y\,k_yk_{z_1}\;+\;\mu_z\,(k^2-k_{z_1}^2)}{k_{z_1}(k_x^2+k_y^2)} \tag{10.13}$$

$$\hat{A}^h(k_x,k_y) \;=\; \frac{k_1^2}{4\pi}\,\frac{-\mu_x\,k_y\;+\;\mu_y\,k_x}{k_{z_1}(k_x^2+k_y^2)}\;, \tag{10.14}$$

where we used the Cartesian components $\boldsymbol{\mu} = (\mu_x, \mu_y, \mu_z)$ for the dipole moment. Finally, introducing the expressions for $\hat{A}^e$ and $\hat{A}^h$ into Eq. (10.10) and using the definition Eq. (10.1) the s-polarized and p-polarized parts of the dyadic Green's function can be determined. The decomposition of the matrix $\overleftrightarrow{\mathbf{M}}$ turns out to be

$$\begin{aligned}
\overleftrightarrow{\mathbf{M}}^s \;&=\; \frac{1}{k_{z_1}(k_x^2+k_y^2)}\begin{bmatrix} k_y^2 & -k_xk_y & 0\\ -k_xk_y & k_x^2 & 0\\ 0 & 0 & 0\end{bmatrix}\\
\overleftrightarrow{\mathbf{M}}^p \;&=\; \frac{1}{k_1^2(k_x^2+k_y^2)}\begin{bmatrix} k_x^2k_{z_1} & k_xk_yk_{z_1} & \mp k_x(k_x^2+k_y^2)\\ k_xk_yk_{z_1} & k_y^2k_{z_1} & \mp k_y(k_x^2+k_y^2)\\ \mp k_x(k_x^2+k_y^2) & \mp k_y(k_x^2+k_y^2) & (k_x^2+k_y^2)^2/k_{z_1}\end{bmatrix}
\end{aligned} \tag{10.15}$$

*Notice, that only $\mathbf{A}^e$ has the units of a vector potential. $\mathbf{A}^h$ is the magnetic analogue of the vector potential.

## 10.3 Dyadic Green's functions for the reflected and transmitted fields

Let us assume that the dipole whose primary field is represented by $\overleftrightarrow{\mathbf{G}}_o$ is located above a planarly layered interface as shown in Fig. 10.1. We choose a coordinate system with origin on the topmost interface. Then, the $z$-coordinate of the dipole ($z_o$) denotes the height of the dipole above the layered medium. To calculate the dipole's reflected field we simply multiply the individual plane waves in $\overleftrightarrow{\mathbf{G}}$ with the corresponding (generalized) Fresnel reflection coefficients $r^s$ and $r^p$. These coefficients are easily expressed as functions of $(k_x, k_y)$ [c.f. Eqs. (**??**), (**??**)]. For the reflected field we obtain the new dyadic Green's function

$$\boxed{\begin{aligned}
\overleftrightarrow{\mathbf{G}}_{ref}(\mathbf{r},\mathbf{r}_o) &= \frac{i}{8\pi^2}\int\!\!\int_{-\infty}^{\infty}\left[\overleftrightarrow{\mathbf{M}}^{s}_{ref}+\overleftrightarrow{\mathbf{M}}^{p}_{ref}\right]\mathrm{e}^{i\left[k_x(x-x_o)+k_y(y-y_o)+k_{z_1}(z+z_o)\right]}\,dk_x\,dk_y \\
\overleftrightarrow{\mathbf{M}}^{s}_{ref} &= \frac{r^s(k_x,k_y)}{k_{z_1}(k_x^2+k_y^2)}\begin{bmatrix} k_y^2 & -k_xk_y & 0 \\ -k_xk_y & k_x^2 & 0 \\ 0 & 0 & 0 \end{bmatrix} \\
\overleftrightarrow{\mathbf{M}}^{p}_{ref} &= \frac{-r^p(k_x,k_y)}{k_1^2(k_x^2+k_y^2)}\begin{bmatrix} k_x^2k_{z_1} & k_xk_yk_{z_1} & k_x(k_x^2+k_y^2) \\ k_xk_yk_{z_1} & k_y^2k_{z_1} & k_y(k_x^2+k_y^2) \\ -k_x(k_x^2+k_y^2) & -k_y(k_x^2+k_y^2) & -(k_x^2+k_y^2)^2/k_{z_1} \end{bmatrix}
\end{aligned}} \tag{10.16}$$

The electric field in the upper half-space is now calculated by the sum of the primary Green's function and the reflected Green's function as

$$\mathbf{E}(\mathbf{r}) \;=\; \omega^2\mu_o\mu_1\left[\overleftrightarrow{\mathbf{G}}_o(\mathbf{r},\mathbf{r}_o)+\overleftrightarrow{\mathbf{G}}_{ref}(\mathbf{r},\mathbf{r}_o)\right]\boldsymbol{\mu}\,. \tag{10.17}$$

The sum of $\overleftrightarrow{\mathbf{G}}$ and $\overleftrightarrow{\mathbf{G}}_{ref}$ can be regarded as the new Green's function of the upper half-space.

The transmitted field can be expressed in terms of the Fresnel transmission coefficients $t^s$ and $t^p$ [c.f. Eqs. (**??**), (**??**)]. For the lower half-space we obtain

$$\overleftrightarrow{\mathbf{G}}_{tr}(\mathbf{r},\mathbf{r}_o) = \frac{i}{8\pi^2}\int_{-\infty}^{\infty}\int\Big[\overleftrightarrow{\mathbf{M}}^{s}_{tr}+\overleftrightarrow{\mathbf{M}}^{p}_{tr}\Big]\mathrm{e}^{i\left[k_x(x-x_o)+k_y(y-y_o)-k_{z_n}(z+\delta)+k_{z_1}z_o\right]}dk_x\,dk_y$$

$$\overleftrightarrow{\mathbf{M}}^{s}_{tr} = \frac{t^s(k_x,k_y)}{k_{z_1}(k_x^2+k_y^2)}\begin{bmatrix} k_y^2 & -k_xk_y & 0\\ -k_xk_y & k_x^2 & 0\\ 0 & 0 & 0\end{bmatrix} \tag{10.18}$$

$$\overleftrightarrow{\mathbf{M}}^{p}_{tr} = \frac{t^p(k_x,k_y)}{k_1k_n(k_x^2+k_y^2)}\begin{bmatrix} k_x^2k_{z_n} & k_xk_yk_{z_n} & k_x(k_x^2+k_y^2)k_{z_n}/k_{z_1}\\ k_xk_yk_{z_n} & k_y^2k_{z_n} & k_y(k_x^2+k_y^2)k_{z_n}/k_{z_1}\\ k_x(k_x^2+k_y^2) & k_y(k_x^2+k_y^2) & (k_x^2+k_y^2)^2/k_{z_1}\end{bmatrix}$$

The parameter $\delta$ denotes the total height of the layered interface. In case of a single interface $\delta=0$. The electric field in the lower half-space is calculated as

$$\mathbf{E}(\mathbf{r}) \;=\; \omega^2\mu_o\mu_1\;\overleftrightarrow{\mathbf{G}}_{tr}(\mathbf{r},\mathbf{r}_o)\,\boldsymbol{\mu}\,. \tag{10.19}$$

The function $\overleftrightarrow{\mathbf{G}}_{tr}$ can be regarded as the new Green's function of the lower half-space.

The calculation of the fields inside the layered structure requires the explicit solution of the boundary conditions at the interfaces. This has been done in Ref. [2] for a two-interface structure (planar layer ontop of a planar substrate) and explicit expressions for the field components can be found in Appendix **??**. The results to be derived here, do not require the knowledge of the fields inside the individual layers. However, to calculte the fields in the upper and lower half-spaces we need to know the generalized Fresnel reflection and transmission coefficients. For a single interface, these coefficients have been stated in Eqs. (**??**), (**??**) and the generalization to multiple interfaces can be found in Ref. [14]. As an example, the reflection and transmission coefficients of a single layer of thickness $d$ read as

$$r^{(p,s)} \;=\; \frac{r_{1,2}^{(p,s)}+r_{2,3}^{(p,s)}\,\exp(2ik_{2z}d)}{1+r_{1,2}^{(p,s)}r_{2,3}^{(p,s)}\,\exp(2ik_{2z}d)} \tag{10.20}$$

$$t^{(p,s)} \;=\; \frac{t_{1,2}^{(p,s)}t_{2,3}^{(p,s)}\,\exp(ik_{2z}d)}{1+r_{1,2}^{(p,s)}r_{2,3}^{(p,s)}\,\exp(2ik_{2z}d)}\,, \tag{10.21}$$

where $r_{i,j}^{(p,s)}$ and $t_{i,j}^{(p,s)}$ are the reflection and transmission coefficients for the single interface $(i,j)$.

In order to calculate the fields in the upper and lower half-spaces it is necessary to transform the expressions for the fields into a cylindrical system. By using the

mathematical identities in Eq. (**??**) it is possible to express the fields in terms of a single integral in $k_\rho$. The magnetic field can be derived by applying Maxwell's equation $i\omega\mu_o\mu_i\mathbf{H}=\nabla\times\mathbf{E}$ which directly leads to

$$\mathbf{H}(\mathbf{r}) = \begin{cases} -i\omega\left[\nabla\times(\overleftrightarrow{\mathbf{G}}+\overleftrightarrow{\mathbf{G}}_{ref})\right]\boldsymbol{\mu} & \text{upper half}-\text{space} \\ -i\omega\,\mu_1/\mu_n\left[\nabla\times\overleftrightarrow{\mathbf{G}}_{tr}\right]\boldsymbol{\mu} & \text{lower half}-\text{space} \end{cases} \tag{10.22}$$

Here, the curl operator acts seprately on each column vector of the dydic Green's functions.

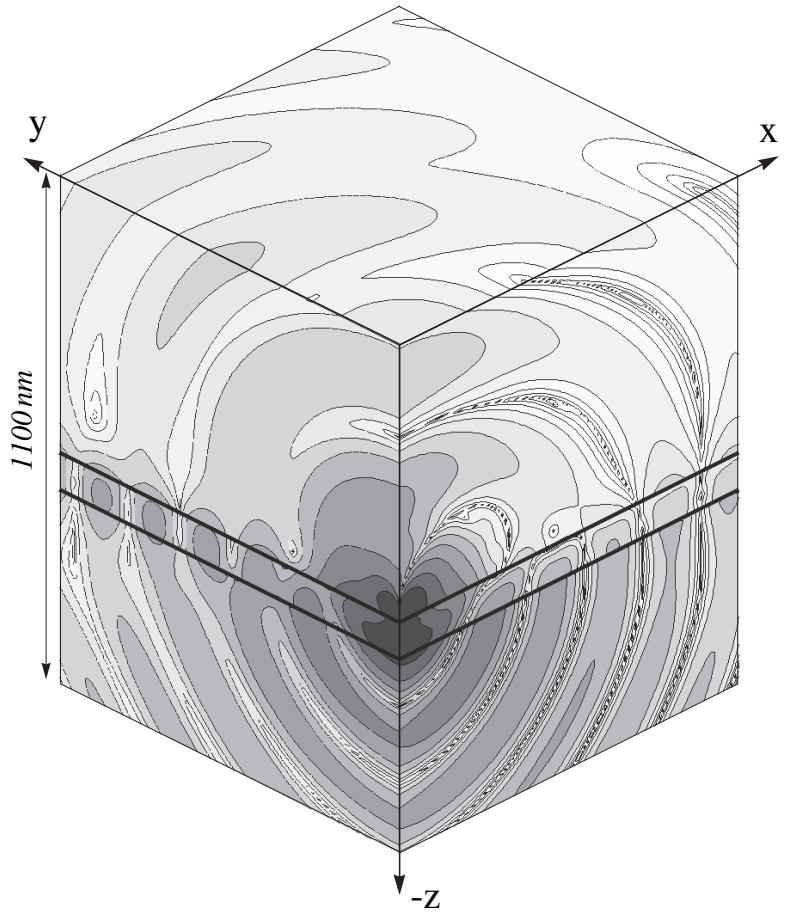


Figure 10.3: Power density of a dipole above a slab waveguide depicted at a certain time. The dipole is located at $h=20nm$ and its axis is in the $(x,z)$ plane. $\vartheta=60°$, $\lambda=488\,nm$, $d=80\,nm$, $\varepsilon_1=1$, $\varepsilon_2=5$, $\varepsilon_3=2.25$. Factor of 2 between successive contourlines.

As an example, Fig. 10.3 shows the field distribution of a dipole in close proximity to a slab waveguide. The dipole is oriented at $\theta = 60°$ in the $(x, z)$ plane, i.e. $\boldsymbol{\mu} = \mu(\sqrt{3}/2, 0, 1/2)$, and radiates predominantly into the lower, optically denser medium. The dipole's near-field excites the two lowest modes, $TE_0$ and $TM_0$, in the waveguide.

## 10.4 Decay rates near planar interfaces

The normalized rate of energy dissipation $P/P_o$ of a radiating dipole is defined by Eq. (**??**). Usually, not all of the dipole's energy is transformed into radiation since it can be coupled to other modes supported by the layered structure (phonons, heat, surface modes, waveguide modes, etc.). For an incoherently decaying quantum system with intrinsic quantum yield $q_i = 1$, the normalized decay rate $\gamma/\gamma_o$ is identical with $P/P_o$ [c.f. Eq. (**??**)] and requires the evaluation of the scattered field $\mathbf{E}_s(\mathbf{r}_o)$ at the dipole's origin $\mathbf{r}_o$. In the present situation the scattered field corresponds to the reflected field $\mathbf{E}_{ref}$ which, at it's origin, reads as

$$\mathbf{E}_{ref}(\mathbf{r}_o) \;=\; \omega^2 \mu_o \mu_1 \, \vec{\mathbf{G}}_{ref}(\mathbf{r}_o, \mathbf{r}_o)\, \boldsymbol{\mu}\,. \tag{10.23}$$

$\vec{\mathbf{G}}_{ref}$ is defined by Eq. (10.16. It is convenient to perform the substitutions

$$k_x = k_\rho \cos\phi, \quad k_y = k_\rho \sin\phi, \quad dk_x dk_y = k_\rho dk_\rho d\phi\,, \tag{10.24}$$

which allow us to solve the integral over $\phi$ analytically. † Evaluated at it's origin, $\vec{\mathbf{G}}_{ref}$ takes on the diagonal form

$$\vec{\mathbf{G}}_{ref}(\mathbf{r}_o, \mathbf{r}_o) \;=\; \frac{i}{8\pi k_1^2} \int_0^\infty \frac{k_\rho}{k_{z_1}} \begin{bmatrix} k_1^2 r^s - k_{z_1}^2 r^p & 0 & 0 \\ 0 & k_1^2 r^s - k_{z_1}^2 r^p & 0 \\ 0 & 0 & 2k_\rho^2 r^p \end{bmatrix} \mathrm{e}^{2ik_{z_1} z_o}\, dk_\rho\,. \tag{10.25}$$

Together with Eq. (10.23) and Eq. (**??**) it is now straightfoward to determine the normalized rate of energy dissipation. For convenience, we perform the substitutions $s = k_\rho/k_1$ and $\sqrt{1-s^2} = k_{z_1}/k_1$. Then, using the abbreviation $s_z = (1-s^2)^{1/2}$ we obtain

$$\boxed{\begin{aligned} \frac{P}{P_o} \;=\; 1 \;+\; \frac{\mu_x^2+\mu_y^2}{p^2}\,\frac{3}{4} \int_0^\infty \mathrm{Re}\left\{ \frac{s}{s_z}\left[r^s - s_z^2 r^p\right]\, \mathrm{e}^{2ik_1 z_o s_z} \right\} ds \\ +\; \frac{\mu_z^2}{p^2}\,\frac{3}{2} \int_0^\infty \mathrm{Re}\left\{ \frac{s^3}{s_z}\, r^p\, \mathrm{e}^{2ik_1 z_o s_z} \right\} ds \end{aligned}} \tag{10.26}$$

†Notice the difference to Eq. (**??**) which was arrived at by transforming a planar surface to a spherical surface. Here, the integration is fixed to a planar surface.

Here, the reflection coefficients are functions of the variable $s$, i.e. $r^s(s)$ and $r^p(s)$. The integration range $[0\,..\,\infty]$ can be divided into the two intervals $[0\,..\,1]$ and $[1\,..\,\infty]$. The first interval is associated with the plane waves of the angular spectrum, i.e. $k_\rho = [0\,..\,k_1]$, whereas the second interval corresponds to the spectrum of evanescent waves $k_\rho = [k_1\,..\,\infty]$. Thus, the dipole interacts with its own reflected plane waves and reflected evanescent waves. The exponential term in the integrands is an exponentially decaying function for evanescent waves, whereas it is oscillatory for plane waves.

According to Eq. (**??**) the normalized rate of energy dissipation is identical with the spontaneous decay rate. Fig. 10.5 shows the normalized molecular lifetime $\tau/\tau_o = (P/P_o)^{-1}$ as a function of the separation $h$ between a substrate and an approaching interface (c.f. Fig. 10.4). The normalization ($\tau_o$) refers to the situation, for which the molecule is located on the glass surface, but the second interface is absent ($h \to \infty$).

The undulations originate from the interference between the propagating fields (plane waves) of the molecule and the reflected fields from the approaching interface. As expected, the undulations are more emphasized for the metal interface and for horizontal dipole orientation. At small $h$, it can be observed that molecular lifetimes for all configurations decrease. This reduction is caused by the increasing nonradiative decay rate mediated by evanescent field components. Depending whether the approaching interface is metallic or dielectric, the evanescent field components of the molecule are thermally dissipated or partly converted to fields propagating at supercritical angles in the upper half-space [15]. For the metal interface the lifetime tends to zero [16] as $h \to 0$. In this case, the molecule transfers its excitation energy to the metal and there is no apparent radiation. As a consequence, the fluorescence is

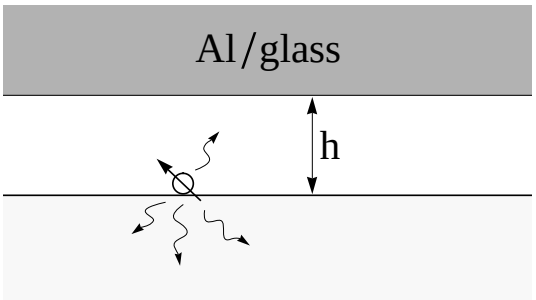


Figure 10.4: Single molecule fluorescence near planar interfaces. The molecule is located on the surface of a dielectric substrate and a metal ($\varepsilon = -34.5 + i\,8.5$) or a glass ($\varepsilon = 2.25$) interface is approached from above. The applied wavelength is $\lambda = 488nm$.

quenched.

Figs. 10.5b,d depict the lifetimes for $h < 20nm$, the distances relevant for near-field optical experiments. For the vertically oriented dipoles the lifetimes are always larger in the case of the dielectric interface. This is not so for the horizontal dipole orientation, where the two curves intersect. Above $h \approx 8.3nm$ the lifetime of an excited molecule faced by an aluminum interface is higher than in the case of a dielectric interface, but lower for separations below $h \approx 8.3nm$. This lifetime reversal can be transferred to the experimental situation in aperture near-field optical microscopy: a molecule at center position of the optical probe is faced by the dielectric core which can be approximated by a planar dielectric interface. For positions below the metal cladding, the situation corresponds to a molecule faced by a planar aluminum in-

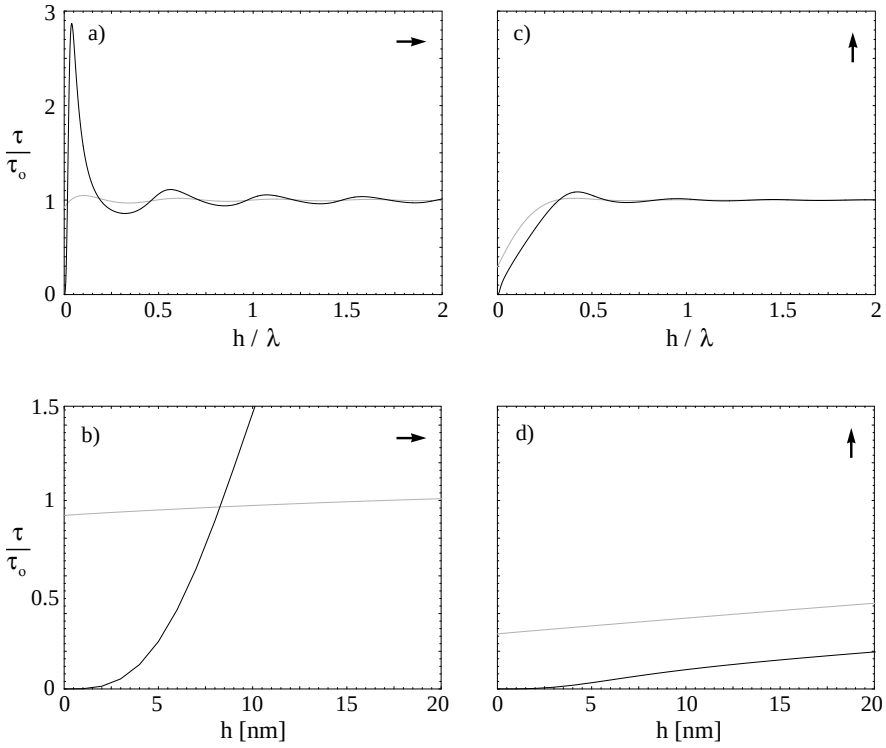


Figure 10.5: Molecular lifetime as a function of the gap $h$. The dark curves were obtained for an approaching metal interface whereas the bright curves refer to an approaching dielectric interface. The arrows indicate the orientation of the dipole axes. The lower figures are close-ups of the upper ones. The normalization with $\tau_o$ corresponds to $h \to \infty$.

terface. Thus, for small probe-sample separations, the lifetime of a molecule with horizontal dipole axis is higher at center position than at displaced positions. The contrary is valid for gaps larger than $\approx 8.3nm$. These findings verify experimental observations [17] and reproduce the numerical results reported in Ref. [18].

The point $h$ at which the curves intersect, depends on the wavelength of the illuminating light and on the orientation of the dipole axis. For longer wavelengths, aluminum behaves more metallic, which shifts the intersection point to larger $h$. At $\lambda = 800nm$, the dielectric constant of aluminum is $\varepsilon = -63.5 + i\,47.3$ and the intersection point appears at $h \approx 14.6nm$.

If a molecule is faced by a finite sized object the lateral symmetry is lost and additional effects will occur at the rims of the objects. The results depend on the relative orientation of the dipole axis with respect to the rims [19, 20].

## 10.5 Farfields

In many situations dipoles near a planarly layered interface are observed in the farfield zone. To understand how the fields are mapped from the near-field to the farfield we need to derive explicit expressions for the asymptotic fields. The radiation condition usually requires that these fields decay as $r^{-1}$. However, it turns out to be a philosophical problem to define fields at an infinite distance from an infinitely extended object. Furthermore, the existence of closed asymptotic expressions is questionable for reasons of energy conservation: fields which propagate along the layered structure, i.e., guided or surface waves, have to decay as $r^{-1/2}$. Regions between the $r^{-1}$ and the $r^{-1/2}$ zones should show transitive behavior. Thus, it could be concluded that no closed far-field expressions exist for stratified media since the decay of the fields depends on the direction of propagation. Nevertheless, closed expressions for the far-field can be derived if the lateral directions, i.e., the regions very close to the layers, are excluded.

One of the advantages of using the angular spectrum representation is the simple and straightforward derivation of the farfield. We have learned in Section **??** that the farfield $\mathbf{E}_\infty$ observed in the direction of the dimensionless unit vector

$$\mathbf{s} \;=\; (s_x, s_y, s_z) \;=\; (\frac{x}{r}, \frac{y}{r}, \frac{z}{r}) \tag{10.27}$$

is determined by the Fourier spectrum $\hat{\mathbf{E}}$ at $z = 0$ as

$$\mathbf{E}_\infty(s_x, s_y, s_z) \;=\; -ik\, s_z\, \hat{\mathbf{E}}(ks_x, ks_y;\, 0)\, \frac{\mathrm{e}^{ikr}}{r}\;. \tag{10.28}$$

This equation requires that we express the wavevector $\mathbf{k}$ in terms of the unit vector $\mathbf{s}$. Since we have different optical properties in the upper and lower half space we use the following definitions

$$\mathbf{s} \;=\; \begin{cases} (\frac{k_x}{k_1}, \frac{k_y}{k_1}, \frac{k_{z1}}{k_1}) & z > 0 \\ (\frac{k_x}{k_n}, \frac{k_y}{k_n}, \frac{k_{zn}}{k_n}) & z < 0 \end{cases} \quad . \tag{10.29}$$

The field $\mathbf{E}$ in upper and lower half-space is determined by the Green's functions $\overleftrightarrow{\mathbf{G}}_o$, $\overleftrightarrow{\mathbf{G}}_{ref}$, and $\overleftrightarrow{\mathbf{G}}_{tr}$ which already are in the form of an angular spectrum [Eqs. (10.6), (10.16), (10.18)]. We can establish the asymptotic farfield forms of the different Green's functions by using the receipe of Eq. (10.28). All there is to be done is to identify the Fourier spectrum of the Green's functions and to carry out the algebra. The resulting expressions are given in Appendix **??**.

In order to have a simple representation of the farfield we choose the origin of the coordinate system on the surface of the uppermost layer such that the dipole is located on the $z$-axis, i.e.

$$(x_o, y_o) \;=\; (0, 0)\,. \tag{10.30}$$

Furthermore, we represent the field in terms of spherical vector coordinates $\mathbf{E} = (E_r, E_\theta, E_\phi)$ by using the spherical angles $\theta, \phi$. It is important to use the correct signs in the substitutions: in the upper half-space we have $s_z = k_{z_1}/k_1 = \cos\theta$, whereas in

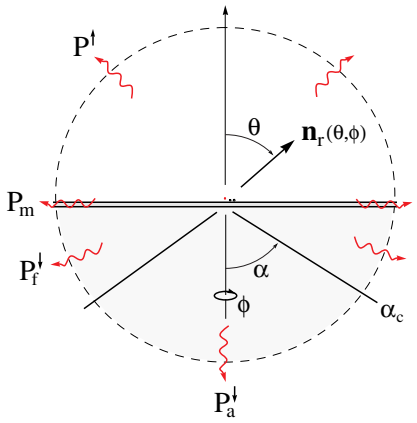


Figure 10.6: Definition of angles used for the asymptotic farfields. The radiated power is split into the contributions $P^\uparrow$ (radiation into upper half-space), $P_a^\downarrow$ (radiation into allowed zone), $P_f^\downarrow$ (radiation into forbidden zone), and $P_m$ (radiation dissipated in the layered medium). The total rate of energy dissipation is satisfies $P = P^\uparrow + P_a^\downarrow + P_f^\downarrow + P_m + P_i$, with $P_i$ being the intrinsically dissipated power.

the lower half-space the relationship is $s_z = k_{z_n}/k_n = -\cos\theta$. For simpler notation it is convenient to define

$$\tilde{s}_z = \frac{k_{z_1}}{k_n} = \sqrt{(n_1/n_n)^2 - (s_x^2 + s_y^2)} \;=\; \sqrt{(n_1/n_n)^2 - \sin^2\theta}\,, \tag{10.31}$$

where $n_1$ and $n_n$ are the refractive indices of upper and lower half-space, respectively. Using the index $j \in [1, n]$ to distinguish between upper and lower half-spaces, the farfield can be represented as

$$\mathbf{E} \;=\; \begin{bmatrix} E_\theta \\ E_\phi \end{bmatrix} \;=\; \frac{k_1^2}{4\pi\varepsilon_o\varepsilon_1}\,\frac{\exp(ik_j r)}{r}\,\begin{bmatrix} [\mu_x\cos\phi + \mu_y\sin\phi]\cos\theta\,\Phi_j^{(2)} \;-\; \mu_z\sin\theta\,\Phi_j^{(1)} \\ -[\mu_x\sin\phi - \mu_y\cos\phi]\,\Phi_j^{(3)} \end{bmatrix} \tag{10.32}$$

with

$$\Phi_1^{(1)} \;=\; \left[e^{-ik_1 z_o\cos\theta} \;+\; r^p(\theta)\,\mathrm{e}^{ik_1 z_o\cos\theta}\right] \tag{10.33}$$

$$\Phi_1^{(2)} \;=\; \left[e^{-ik_1 z_o\cos\theta} \;-\; r^p(\theta)\,\mathrm{e}^{ik_1 z_o\cos\theta}\right] \tag{10.34}$$

$$\Phi_1^{(3)} \;=\; \left[e^{-ik_1 z_o\cos\theta} \;+\; r^s(\theta)\,\mathrm{e}^{ik_1 z_o\cos\theta}\right] \tag{10.35}$$

$$\Phi_n^{(1)} \;=\; \frac{n_n}{n_1}\,\frac{\cos\theta}{\tilde{s}_z(\theta)}\;t^p(\theta)\,\mathrm{e}^{ik_n[z_o\tilde{s}_z(\theta)\,+\,\delta\cos\theta]} \tag{10.36}$$

$$\Phi_n^{(2)} \;=\; -\frac{n_n}{n_1}\,t^p(\theta)\,\mathrm{e}^{ik_n[z_o\tilde{s}_z(\theta)\,+\,\delta\cos\theta]} \tag{10.37}$$

$$\Phi_n^{(3)} \;=\; \frac{\cos\theta}{\tilde{s}_z(\theta)}\;t^s(\theta)\,\mathrm{e}^{ik_n[z_o\tilde{s}_z(\theta)\,+\,\delta\cos\theta]}\,. \tag{10.38}$$

A vertically oriented dipole is described by the potential $\Phi_j^{(1)}$, whereas a horizontal dipole is represented by $\Phi_j^{(2)}$ and $\Phi_j^{(3)}$ containing the amount of $p$-polarized and $s$-polarized light, respectively. Let us first discuss the farfields in the upper half-space. To understand the potentials $\Phi_1^{(1)} \;-\; \Phi_1^{(3)}$ we analyze the farfield of a dipole in a homogeneous medium. We displace the dipole from the coordinate origin by a distance $z_o$ along the $z$-axis. According to Eq. (**??**) the electric field in the far-zone is defined by the term $\exp(ik_1R)/R$. However, the radial coordinate $R$ is measured from the origin of the dipole and not from the coordinate origin. If we designate the latter by $r$ we can write

$$R \;=\; r\sqrt{1 + \frac{z_o^2 - 2z_o r\cos\vartheta}{r^2}} \;\approx\; r - z_o\cos\theta\,. \tag{10.39}$$

Only the first two terms in the series expansion of the square root have been retained. It is important to include the second term in the phase of the wave in order to

account for the phase delay. On the other hand, the second term is meaningless for the amplitude since $r \gg z_o$. Thus, we can write

$$\frac{\mathrm{e}^{ik_1 R}}{R} \;=\; \frac{\mathrm{e}^{ik_1 r}}{r}\,\mathrm{e}^{-ik_1 z_o \cos\theta}\;, \tag{10.40}$$

which is known as the Fraunhofer approximation. By comparison we find that the first term in the potentials $\Phi_1^{(1)} - \Phi_1^{(3)}$ corresponds to direct dipole radiation. The exponential factor of the second term has a minus sign in the exponent. Therefore, the second term can be identified as radiation from a dipole located a distance $z_o$ beneath the top surface of the layered medium. The magnitude of this image dipole is weighted by the Fresnel reflection coefficients. This is a remarkable result: in the farfield, a dipole near a layered medium radiates as the superposition of two dipole fields, namely its own field and the field of its image dipole.

The expressions for the transmitted farfield are more complicated. This arises through the term $\tilde{s_z}$ defined in Eq. (10.31). Depending on the optical properties of upper and lower half-spaces, this term can be either real or imaginary. In fact, in many cases the lower half-space (substrate) is optically denser than the upper one. In these situtions $\tilde{s_z}$ becomes imaginary for the angular range $\theta = [\pi/2 \ldots arcsin(n_1/n_n)]$ which exactly corresponds to the forbidden zone discussed before. In the forbidden zone, the exponential factor in the potentials $\Phi_n^{(1)} - \Phi_n^{(3)}$ becomes an exponentially decaying function. Therefore, for separations $z_o \gg \lambda$ there is no light coupled into the forbidden zone. On the other hand, in the angular range $\theta = [arcsin(n_1/n_n) \ldots \pi]$ (allowed zone) the dipole radiation does not depend on the height of the dipole as we shall see in the next section.

## 10.6 Radiation patterns

In the farfield, the magnetic field vector is transverse to the electric field vector and the time averaged Poynting vector is calculated as

$$\langle \mathbf{S} \rangle \;=\; \frac{1}{2}\,\mathrm{Re}\{\mathbf{E} \times \mathbf{H}^*\} \;=\; \frac{1}{2}\sqrt{\frac{\varepsilon_o \varepsilon_j}{\mu_o \mu_j}}\;\mathbf{E}\cdot\mathbf{E}^*\,\mathbf{n}_r\;, \tag{10.41}$$

with $\mathbf{n}_r$ being the unit vector in radial direction. The radiated power per unit solid angle $d\Omega = \sin\theta\, d\theta\, d\phi$ is

$$P \;=\; p(\Omega)\,d\Omega \;=\; r^2\,\langle \mathbf{S} \rangle \cdot \mathbf{n}_r\;, \tag{10.42}$$

where $p(\Omega) = p(\theta, \phi)$ is defined as the radiation pattern. With the farfield in Eq. (10.32) and the corresponding potentials it is straightforward to calculate the normalized radiation patterns as

$$\frac{p(\theta,\phi)}{P_o} = \frac{3}{8\pi}\frac{\varepsilon_j}{\varepsilon_1}\frac{n_1}{n_j}\frac{1}{|\boldsymbol{\mu}|^2}\left[\mu_z^2\sin^2\theta\left|\Phi_j^{(1)}\right|^2 + [\mu_x\cos\phi+\mu_y\sin\phi]^2\cos^2\theta\left|\Phi_j^{(2)}\right|^2 + [\mu_x\sin\phi-\mu_y\cos\phi]^2\left|\Phi_j^{(3)}\right|^2 - \mu_z[\mu_x\cos\phi+\mu_y\sin\phi]\,\cos\theta\,\sin\theta\left[\Phi_j^{*(1)}\,\Phi_j^{(2)} + \Phi_j^{(1)}\,\Phi_j^{*(2)}\right]\right] \quad (10.43)$$

Here, $P_o$ corresponds to the total rate of energy dissipation in a homogeneous (unbounded) medium characterized by $\varepsilon_1, \mu_1$ [c.f. Eq. (**??**)]. The first term in the brackets of Eq. (10.43) contains the $p$-polarized contribution of the vertical orientation, whereas the second and third term contain the $p$- and $s$-polarized contributions of the horizontal orientation. Of particular interest is the fourth term which originates from interferences between the $p$-polarized terms of the two major orientations. Thus, the $p$-polarized light of a vertical and a horizontal dipole, which are located at the same point, interfere if the two dipoles radiate coherently. The radiation patterns for arbitrary dipole orientation usually cannot be put together additively. Notice however,

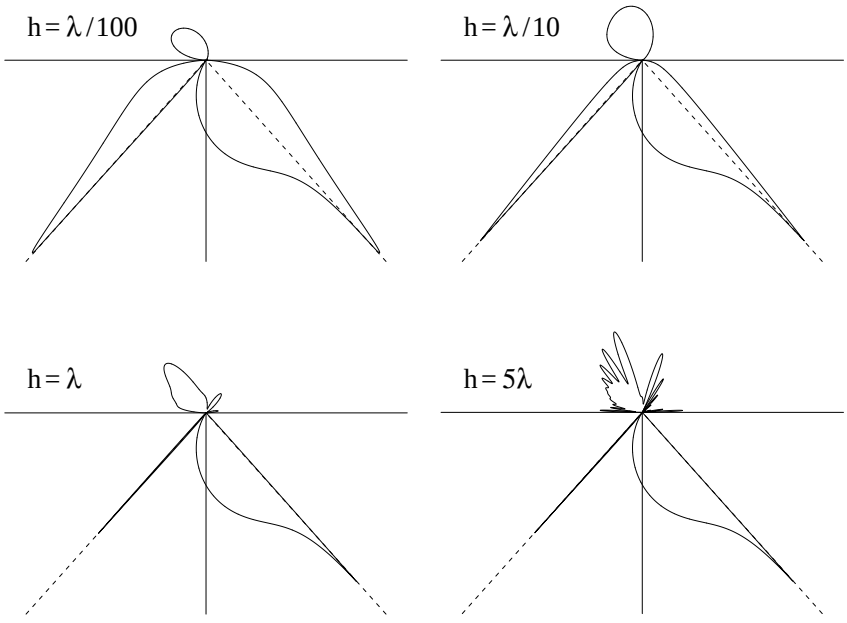


Figure 10.7: Radiation patterns of a dipole with orientation $\vartheta = 60°$ approaching a planar waveguide. $\lambda = 488\,nm$, $\delta = 80\,nm$, $\varepsilon_1 = 1$, $\varepsilon_2 = 5$, $\varepsilon_3 = 2.25$. The different heights $z_o = h$ of the dipole are indicated in the figure. The radiation patterns are shown in the plane defined by the dipole axis and the $z$-axis. Note that the *allowed light* does not depend on $h$ and that the *forbidden light* is always symmetrical with respect to the vertical axis.

that upon integration over $\varphi$, the interference term cancels out.

Eq. (10.43) allows us to determine the radiation patterns of a dipole near an arbitrarily layered system; in the special case of a single interface it reproduces the formulas obtained by Lukosz [15, 21]. As an illustration, Fig. 10.7 shows the radiation patterns of a dipole near a slab waveguide. The radiation in the forbidden zone depends exponentially on the height $z_o$ of the dipole whereas the radiation in the allowed zone does not depend on $z_o$. In the lower half-space the interference term in Eq. (10.41) reads as

$$\left[\Phi_j^{*(1)}\,\Phi_j^{(2)} + \Phi_j^{(1)}\,\Phi_j^{*(2)}\right] \propto \left|t^{(p)}(\theta)\right|^2 \mathrm{e}^{-2\,z_o\,\mathrm{Im}\{\tilde{s}_z(\theta)\}}\ \mathrm{Re}\left\{\frac{\cos\theta}{\tilde{s}_z(\theta)}\right\}\ . \tag{10.44}$$

In the forbidden zone, $\tilde{s_z}$ is imaginary and the interference term vanishes. Thus, the waves of a vertical and a horizontal dipole at the same position do not interfere in the forbidden zone and the radiation patterns will always be symmetric with respect to $\phi$. This rather surprising result was already found by Lukosz in Ref.[21] for the case of a single interface. Recently, the radiation patterns of Eq. (10.43) have been confirmed for a single molecule near a dielectric interface [22]. It is remarkable that although a single photon is emitted at a time all the interference terms in Eq. (**??**) are retained. Thus, as is well known, the photon travels many paths simultaneously and all the different paths interfere giving rise to the predicted dipole radiation patterns. Fig. 10.8 shows the radiation pattern of a single molecule placed near a glass surface.

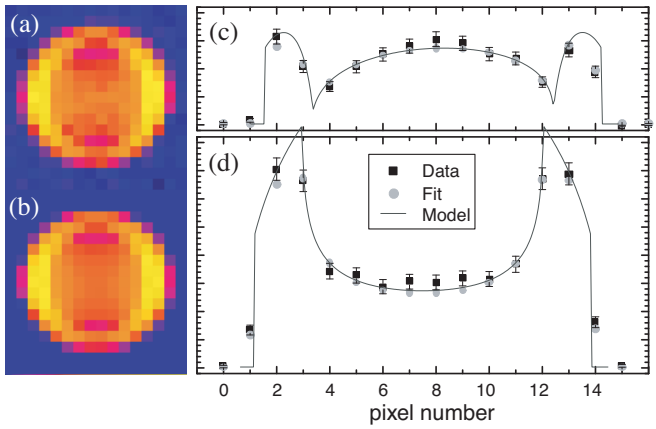


Figure 10.8: Radiation pattern of a single molecule located near a glass surface. The pattern reflects the photons emitted into the dielectric and imaged onto a CCD with a $NA = 1.4$ objective lens. (a) Data, (b) fitted pattern using Eq. (10.43), (c,d) cross-sections along a horizontal and a vertical line through the center of the pattern, respectively. From [22].

The pattern has been recorded with a CCD and is compared with the calculated pattern according Eq. (10.43).

Fig. 10.9 shows the angular radiation pattern of a dipole near a single dielectric interface. These patterns are evaluated at different distances $r$ from the dipole's origin and compared with the farfield pattern calculated according Eq. (10.43). It can be recognized that for certain angles $\theta$ the fields converge rather slowly towards the analytical farfields. The critical direction is the critical angle of total internal reflection. Light coupled into this angle is generated by dipole fields that propagate parallel to the layered system. These fields refract at the surface at an infinite lateral distance. Thus, reducing the infinite extension of the layered system will influence the farfield mainly near the critical angle. The phases of the spherical waves of upper and lower half-space are not identical on the interface. Thus, close to the interface other wave forms must exist in order to compensate for the phase mismatch. In the literature these waves are known as *lateral waves*. Lateral waves decay by radiation into the critical angle of total internal reflection (TIR). In the case of a plane interface illuminated under TIR conditions, lateral waves explain the lateral displacement between incident and reflected beam (Goos-Hänchen shift). Besides lateral waves, a layered medium can also support guided waves. These modes decay as $r^{-1/2}$. Thus, the decay of guided waves is even slower than the $r^{-1}$ decay of the derived farfield. Because these modes decrease exponentially into the two half spaces they are only visible in the lateral direction $\theta = \pi/2$. In the very farfield Eqs. (10.32) - (10.38) are correct, since lateral waves decay faster ($r^{-2}$) than spherical waves, and since the direction $\theta = \pi/2$ is not considered.

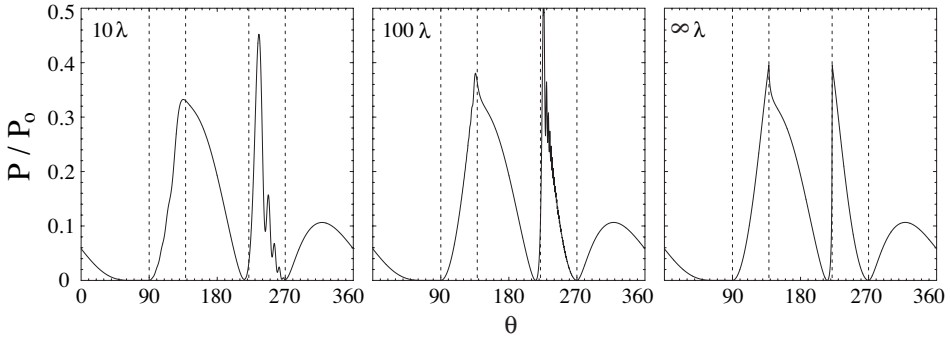


Figure 10.9: Angular distribution of power radiated from a dipole with orientation $\vartheta = 60°$ and height $h = 20nm$ above a dielectric half-space. $\lambda = 633nm$, $\varepsilon_1 = 1$, $\varepsilon_2 = 2.25$. The radiation patterns are shown for different distances from the dipole's origin and are depicted in the $(x, z)$-plane. The lower half space corresponds to $90° < \theta < 270°$. The interface and the critical angle are shown as dashed vertical lines.

## 10.7 Where is the radiation going?

As already discussed in Section **??**, not all of a dipole's dissipated energy is converted into propagating radiation (photons). We have defined the quantum yield $Q$ as the ratio of radiative to total decay rate, i.e. power released as radiation versus the totally dissipated power [c.f. Eq. (**??**)]. However, in an experiment one cannot detect all of the released radiation and hence one defines the *apparent quantum yield* $Q_a$ as the ratio of *detected* power to totally dissipated power. In this section we analyze how much of a dipole's energy is emitted into the upper half-space, lower half-space, and into other modes of radiation (waveguides, surface waves, etc.).

As illustrated in Fig. 10.6 the total rate of energy dissipation is

$$P = P^{\uparrow} + P_a^{\downarrow} + P_f^{\downarrow} + P_m + P_i \ , \tag{10.45}$$

where $P_{\uparrow}$, $P_a^{\downarrow}$, $P_f^{\downarrow}$ are the power radiated into the upper half-space, the allowed zone and the forbidden zone, respectively. $P_m$ denotes the power coupled into the layered medium (waveguide modes, surface modes, thermal losses, etc.) and $P_i$ is the intrinsically dissipated power. The latter is associated with the intrinsic quantum yield $q_i$ defined earlier. In order to derive $P_{\uparrow}$, $P_a^{\downarrow}$, and $P_f^{\downarrow}$, we need to integrate the radiation pattern in Eq. (10.43) over the corresponding angular ranges. It is convenient to use the following substitutions

$$s \ = \ \begin{cases} \sin\theta & z > 0 \\ (n_n/n_1)\sin\theta & z < 0 \ . \end{cases} \tag{10.46}$$

With these substitutions the interval $s = [0\,..\,1]$ defines the plane wave components of the dipole field, whereas the interval $s = [1\,..\,\infty]$ is associated with the dipole's evanescent waves. Furthermore, the different angular ranges are mapped as

$$\begin{aligned} \theta &= [0\,..\,\pi/2] && \rightarrow && s = [0\,..\,1] \\ \theta &= [\pi/2\,..\,\arcsin(n_1/n_n)] && \rightarrow && s = [(n_n/n_1)\,..\,1] \\ \theta &= [\arcsin(n_1/n_n)\,..\,\pi] && \rightarrow && s = [1\,..\,0] \ . \end{aligned} \tag{10.47}$$

Hence, we see that the angular range $\theta = [\pi/2\,..\,\arcsin(n_1/n_n)]$ which corresponds to the forbidden zone is associated with the dipole's evanescent fields. After integration of the radiation pattern in the upper half-space and using the abbreviation $s_z = (1{-}s^2)^{1/2}$

we obtain

$$\frac{P^{\uparrow}}{P_o} = \frac{\mu_x^2+\mu_y^2}{p^2}\left[\frac{1}{2} + \frac{3}{8}\int_0^1 \left[s\,s_z|r^p|^2 + \frac{s}{s_z}|r^s|^2\right]ds - \frac{3}{4}\int_0^1 \mathrm{Re}\left\{\left[s\,s_z r^p - \frac{s}{s_z}r^s\right]\mathrm{e}^{2ik_1 z_o s_z}\right\}ds\right] + \frac{\mu_z^2}{p^2}\left[\frac{1}{2} + \frac{3}{4}\int_0^1 \frac{s^3}{s_z}|r^p|^2\,ds + \frac{3}{2}\int_0^1 \mathrm{Re}\left\{\frac{s^3}{s_z}\,r^p\,\mathrm{e}^{2ik_1 z_o s_z}\right\}ds\right]. \quad (10.48)$$

For both, the horizontal dipole and the vertical dipole, there are three different terms. The first one corresponds to direct dipole radiation: one half of the dipole's primary field is radiated into the upper-half space. The second term corresponds to the power that is reflected from the interface and the last term accounts for interferences between the primary dipole field and the reflected dipole field. It is important to notice, that the integration runs only over the interval $s=[0\,..\,1]$. Therefore, only plane wave components contribute to the radiation into the upper half-space.

To determine radiation into the lower half-space we use the substitution of Eq. refch3141) and integrate over the angular range of the lower half-space. The total radiation in the lower half-space $P^{\downarrow}$ is calculated as

$$\frac{P^{\downarrow}}{P_o} = \frac{3}{8}\,\frac{\mu_x^2+\mu_y^2}{p^2}\,\frac{\varepsilon_n}{\varepsilon_1}\,\frac{n_1}{n_n}\int_0^{n_n/n_1} s\,[1-(\tfrac{n_1}{n_n})^2 s^2]^{1/2}\left[\,|t^p|^2 + |t^s|^2\,|1-s^2|^{-1}\right]\mathrm{e}^{-2k_1 z_o s_z''}\,ds + \frac{3}{4}\,\frac{\mu_z^2}{p^2}\,\frac{\varepsilon_n}{\varepsilon_1}\,\frac{n_1}{n_n}\int_0^{n_n/n_1} s^3\,[1-(\tfrac{n_1}{n_n})^2 s^2]^{1/2}\;|t^p|^2\,|1-s^2|^{-1}\,\mathrm{e}^{-2k_1 z_o s_z''}\,ds\,, \quad (10.49)$$

where $s_z'' = \mathrm{Im}\{(1-s^2)^{1/2}\}$. In the case where $n_n > n_1$ it is possible to separate the angular ranges of the allowed zone and the forbidden zone. The allowed light turns out to be

$$\frac{P_a^{\downarrow}}{P_o} = \frac{3}{8}\,\frac{\mu_x^2+\mu_y^2}{p^2}\,\frac{\varepsilon_n}{\varepsilon_1}\,\frac{n_1}{n_n}\int_0^{1} s\,[1-(\tfrac{n_1}{n_n})^2 s^2]^{1/2}\left[\,|t^p|^2 + |t^s|^2\,(1-s^2)^{-1}\right]ds \quad (10.50)$$
$$+ \frac{3}{4}\,\frac{\mu_z^2}{p^2}\,\frac{\varepsilon_n}{\varepsilon_1}\,\frac{n_1}{n_n}\int_0^{1} s^3\,[1-(\tfrac{n_1}{n_n})^2 s^2]^{1/2}\;|t^p|^2\,(1-s^2)^{-1}\,ds \qquad (n_n > n_1).$$

Similarily, the forbidden light is determined as

$$\frac{P_f^{\downarrow}}{P_o} = \frac{3}{8}\frac{\mu_x^2+\mu_y^2}{p^2}\frac{\varepsilon_n}{\varepsilon_1}\frac{n_1}{n_n}\int_1^{n_n/n_1} s\left[1-(\tfrac{n_1}{n_n})^2 s^2\right]^{1/2}\left[\,|t^p|^2+|t^s|^2\,(s^2-1)^{-1}\right]\mathrm{e}^{-2k_1 z_o\sqrt{s^2-1}}\,ds$$

$$+\frac{3}{4}\frac{\mu_z^2}{p^2}\frac{\varepsilon_n}{\varepsilon_1}\frac{n_1}{n_n}\int_1^{n_n/n_1} s^3\left[1-(\tfrac{n_1}{n_n})^2 s^2\right]^{1/2}|t^p|^2\,(s^2-1)^{-1}\,\mathrm{e}^{-2k_1 z_o\sqrt{s^2-1}}\,ds \qquad (n_n>n_1). \tag{10.51}$$

These expressions demonstrate that the allowed light does not depend on the height of the dipole whereas the forbidden light shows the expected exponential dependence on the dipole's vertical position. Notice, that since $s=k_\rho/k_1$ the term with the square root in the integrands corresponds to $k_{z_n}/k_n$. Assuming that there are no intrinsic losses ($P_i=0$), the power dissipated by the layered medium (thermal losses, waveguide and surface modes) is calculated as

$$P_m = P-(P^{\uparrow}+P^{\downarrow})\,, \tag{10.52}$$

where $P$ is determined by Eq. (10.26). For a lossless layered medium that does not support any waveguide modes it can be demonstrated that $P_m=0$ (c.f. Problem 10.3).

As an illustration of the here developed results Fig. 10.10 displays the different

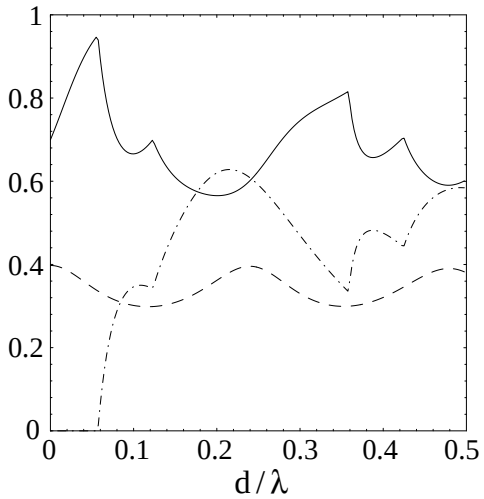


Figure 10.10: Allowed light ($P_a^{\downarrow}$, dashed curve), forbidden light ($P_f^{\downarrow}$, solid curve) and radiation coupled into the waveguide ($P_m=P-P^{\uparrow}-P^{\downarrow}$, dash-dotted curve) as a function of the thickness $d$ of the slab waveguide characterized in Fig. 10.3. The discontinuities correspond to the cut-offs of the $TE_0$, $TM_0$, $TE_1$ and $TM_1$ modes.

radiation terms for a dipole located above the dielectric waveguide shown in Fig. 10.3. The dipole is held at a fixed position $z_o = 80nm$ and the thickness $d$ of the waveguide is varied. While the allowed light is characterized by undulations of periodicity $\pi/k_2$, the forbidden light shows an irregular behavior with discontinuities for certain $d$. The locations of these discontinuities correspond to the cutoff conditions of the waveguide modes. For low $d$ all waveguide modes are beyond cut-off causing that in the time-average no energy is coupled into the waveguide ($P_m = 0$). At $d \approx 0.058\,\lambda$ the fundamental $TE_0$ mode becomes propagating, and a net energy is coupled to the guide. While $d$ is further increased, other modes can be excited as well.

## 10.8 Magnetic dipoles

In the microwave regime paramagnetic materials exhibit magnetic transitions (electron spin resonance). In the infrared small metal particles show magnetic dipole absorption caused by eddy currents of free carriers produced by the magnetic vector of the electromagnetic field. The field of a magnetic dipole in a planarly layered medium is therefore important as well. From a theoretical point of view, these fields are dual to the fields of the electric dipole. The field of a magnetic dipole with moment $\mathbf{m}$ can be derived from the field of an electric dipole moment $\boldsymbol{\mu}$ by simply performing the substitution

$$[\mathbf{E},\, \mathbf{H},\, \mu_o\mu,\, \varepsilon_o\varepsilon,\, \boldsymbol{\mu}] \;\; \rightarrow \;\; [\mathbf{H},\, -\mathbf{E},\, \varepsilon_o\varepsilon,\, \mu_o\mu,\, \mu\mathbf{m}]\,. \tag{10.53}$$

With these substitutions, the reflection coefficients $r^s$ and $r^p$ are also interchanged. Thus, the field of a vertically oriented magnetic dipole will be purely $s$-polarized. In this case, no surface waves will be excited. Note, that the electric dipole moment has the units $[\boldsymbol{\mu}] = Ams$, whereas the units of the magnetic dipole are $[\mathbf{m}] = Am^2$. The power radiated by an electric dipole with moment $\boldsymbol{\mu} = 1$ in a homogeneous medium is $\mu_o\mu\varepsilon_o\varepsilon$ times the power radiated by a magnetic dipole with moment $\mathbf{m} = 1$.

## 10.9 Image dipole approximation

The computational effort can be considerably reduced if retardation can be neglected on the interface. In this case the fields will still satisfy Maxwell's equations in both half-spaces, but the standard static image theory is applied to approximately match the boundary conditions. We will outline the principle of this approximation for a single single interface. Since the electromagnetic field is considered in its static limit ($k \rightarrow 0$) the electric and magnetic fields are decoupled and can be treated separately. For simplicity, only the electric field is considered.

Fig. 10.11 shows an arbitrary oriented dipole above a planar interface and its induced dipole in the medium below. The distance of the image dipole to the interface is the same as for the primary dipole. However, the magnitude of the image dipole moment is different. The static electric field of the primary dipole in the upper half-space reads as

$$\mathbf{E}_{prim} \;=\; -\nabla\phi\,, \qquad with \qquad \phi(\mathbf{r}) \;=\; \frac{1}{4\pi\,\varepsilon_o\,\varepsilon_1}\,\frac{\boldsymbol{\mu}\cdot\mathbf{r}}{r^3}\,. \tag{10.54}$$

The vector $\mathbf{r}$ denotes the radial vector measured from the position of the primary dipole and $r$ is its magnitude. Similarly, the corresponding radial vector of the image dipole is denoted as $\mathbf{r}'$. For simplicity, the dipole moment $\boldsymbol{\mu}$ is decomposed into its parallel and vertical part with respect to the planar interface. Without loss of generality, the parallel component is assumed to point into $x$ direction

$$\boldsymbol{\mu} \;=\; \mu_x\mathbf{n}_x + \mu_z\mathbf{n}_z\,. \tag{10.55}$$

$\mathbf{n}_x$ and $\mathbf{n}_z$ denote the unit vectors in $x$ and $z$ direction, respectively. In the following, the electric field will be considered for each of the two major orientations separately.

### 10.9.1 Vertical dipole

For a dipole $\boldsymbol{\mu} = \mu_z\mathbf{n}_z$, the evaluation of the primary electric field in Eq. (10.54 in cartesian coordinates leads to

$$\mathbf{E}_{prim} \;=\; \frac{\mu_z}{4\pi\,\varepsilon_o\,\varepsilon_1}\left[\frac{3x(z-h)}{r^5},\,\frac{3y(z-h)}{r^5},\,\frac{3(z-h)^2}{r^5}-\frac{1}{r^3}\right]\,, \tag{10.56}$$

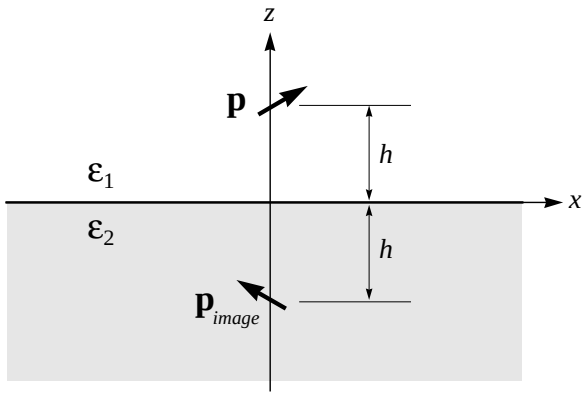


Figure 10.11: Principle of the image dipole approximation. $\boldsymbol{\mu}$ and $\boldsymbol{\mu}_{image}$ denote the primary dipole and the image dipole, respectively. Static image theory is applied to determine the magnitude of $\boldsymbol{\mu}_{image}$.

where $h$ is the height of the dipole above the interface. Assuming an image dipole $\boldsymbol{\mu}=\mu_z \mathbf{n}_z$, a similar expression can be derived for the image field $\mathbf{E}_{image}$

$$\mathbf{E}_{image} = \frac{\mu_z}{4\pi\varepsilon_o\varepsilon_1}\left[\frac{3x(z+h)}{r'^5}, \frac{3y(z+h)}{r'^5}, \frac{3(z+h)^2}{r'^5} - \frac{1}{r'^3}\right], \tag{10.57}$$

where $r'$ denotes the radial distance measured from the location of the image dipole. A reasonable ansatz for the total field $\mathbf{E}$ in either of the two half-spaces is

$$\mathbf{E} = \begin{cases} \mathbf{E}_{prim} + A_v\,\mathbf{E}_{image} & z>0 \\ B_v\,\mathbf{E}_{prim} & z<0 \end{cases}, \tag{10.58}$$

with the two unknown parameters $A_v$ and $B_v$. By requiring the boundary conditions at the interface $z=0$, $A_v$ and $B_v$ can be determined

$$\begin{aligned} A_v &= \frac{\varepsilon_2-\varepsilon_1}{\varepsilon_2+\varepsilon_1} \\ B_v &= \frac{\varepsilon_1}{\varepsilon_2}\frac{2\,\varepsilon_2}{\varepsilon_2+\varepsilon_1}. \end{aligned} \tag{10.59}$$

### 10.9.2 Horizontal dipole

The procedure for a dipole $\boldsymbol{\mu}=\mu_x\mathbf{n}_x$ is similar. The primary and the image field turn out to be

$$\mathbf{E}_{prim} = \frac{\mu_x}{4\pi\varepsilon_o\varepsilon_1}\left[\frac{3x^2}{r^5} - \frac{1}{r^3}, \frac{3xy}{r^5}, \frac{3x(z-h)}{r^5}\right], \tag{10.60}$$

$$\mathbf{E}_{image} = \frac{\mu_x}{4\pi\varepsilon_o\varepsilon_1}\left[\frac{3x^2}{r'^5} - \frac{1}{r'^3}, \frac{3xy}{r'^5}, \frac{3x(z+h)}{r'^5}\right]. \tag{10.61}$$

The corresponding ansatz for the total field $\mathbf{E}$ in either of the two half-spaces is

$$\mathbf{E} = \begin{cases} \mathbf{E}_{prim} + A_h\,\mathbf{E}_{image} & z>0 \\ B_h\,\mathbf{E}_{prim} & z<0 \end{cases}. \tag{10.62}$$

As before, the unknown parameters $A_h$ and $B_h$ can be determined by the boundary conditions at $z=0$

$$\begin{aligned} A_h &= -\frac{\varepsilon_2-\varepsilon_1}{\varepsilon_2+\varepsilon_1} \\ B_h &= \frac{\varepsilon_1}{\varepsilon_2}\frac{2\,\varepsilon_2}{\varepsilon_2+\varepsilon_1}. \end{aligned} \tag{10.63}$$

### 10.9.3 Including retardation

Using the parameters $A_v$, $B_v$, $A_h$ and $B_h$ the magnitude of the image dipole is

$$|\boldsymbol{\mu}_{image}| \;=\; \frac{\varepsilon_2 - \varepsilon_1}{\varepsilon_2 + \varepsilon_1}\,|\boldsymbol{\mu}| \tag{10.64}$$

If the vertical component of $\boldsymbol{\mu}_{image}$ points in the same direction as the vertical component of $\boldsymbol{\mu}$, the horizontal components have different signs. As indicated in Fig. 10.11, the horizontal components of $\boldsymbol{\mu}_{image}$ and $\boldsymbol{\mu}$ point into different directions if their vertical components have the same direction. To obtain the static field in the upper-half space, the fields of the two dipoles $\boldsymbol{\mu}$ and $\boldsymbol{\mu}_{imag}$ have to be superposed. The field in the lower half-space simply corresponds to the attenuated primary dipole field. The attenuation is given by the factor $2\,\varepsilon_2/(\varepsilon_2 + \varepsilon_1)$. Note that the dipoles are considered to be located in the same medium as the point of observation.

So far, the location, orientation and magnitude of the dipole moments $\boldsymbol{\mu}$ and $\boldsymbol{\mu}_{image}$ have been determined. In order to fulfill Maxwell's equations in both half-spaces, the static dipole fields are replaced by their nonretarded forms

$$\mathbf{E} \sim \left[\nabla\,\nabla\cdot\right]\frac{\boldsymbol{\mu}}{r} \qquad \rightarrow \qquad \mathbf{E} \sim \left[k^2 + \nabla\,\nabla\cdot\right]\frac{\boldsymbol{\mu}}{r}\,\mathrm{e}^{ikr}\;. \tag{10.65}$$

Although this substitution rescues Maxwell's equations in both half-spaces it introduces a violation of the boundary conditions. The image dipole approximation therefore has its obvious limitations. In order to keep the errors in bounds, the height $h$ of the primary dipole must be small and the fields may only be evaluated in a limited range from the dipole location. In fact, the image dipole approximation leads to reasonable accuracy as long as short range interactions are considered.

# Problems

**Problem 10.1** Derive Eq. (10.26) and plot the radiative (plane waves), non-radiative (evanescent waves), and total decay rate ($q_i = 1$) as a function of the normalized height $z_o/\lambda$ for the following situations:

1. Horizontal dipole in vacuum above a dielectric substrate ($\varepsilon = 2.25$).
2. Vertical dipole in vacuum above a dielectric substrate ($\varepsilon = 2.25$).
3. Horizontal dipole in vacuum above an aluminum substrate ($\varepsilon = -34.5 + 8.5i$, $\lambda = 488nm$).
4. Vertical dipole in vacuum above an aluminum substrate ($\varepsilon = -34.5 + 8.5i$, $\lambda = 488nm$).

**Problem 10.2** Calculate the normalized energy flux ($P_1^{\downarrow}/P_o$) through a horizontal plane right beneath a dipole which is located above an arbitrary stratified medium. Derive first the magnetic field $\mathbf{H}$ which corresponds to the electric field in Eq. (10.16 and then determine the z-component of the Poynting vector $\langle S_z \rangle$. Use the Bessel function closure relations (c.f. Eq. (**??**) to integrate $\langle S_z \rangle$ over the horizontal plane. Show that the result is identical with $(P - P_1^{\uparrow} - P_n^{\downarrow})/P_o$ as defined in Section 10.7.

**Problem 10.3** Demonstrate that for a dipole near a single dielectric interface the total dissipated power $P$ is identical to the total integrated radiation pattern $P^{\uparrow} + P_a^{\downarrow} + P_f^{\downarrow}$.

Hint: Express the transmission coefficients in terms of the reflection coefficients as

$$\begin{aligned} t^s &= [1+r^s], & (k_{z_n}/k_{z_1})\, t^s &= (\mu_n/\mu_1)\,[1-r^s] \\ t^p &= (\varepsilon_1/\varepsilon_n)(n_n/n_1)\,[1+r^p], & (k_{z_n}/k_{z_1})\, t^p &= (n_n/n_1)\,[1-r^p]\,. \end{aligned}$$

**Problem 10.4** Consider a molecule with an emission dipole moment parallel to an aluminum substrate. The emission wavelength is $\lambda = 488nm$ and the dielectric constant of the substrate is $\varepsilon = -34.5 + 8.5i$. Determine the apparent quantum yield $q_a$ defined as the ratio between the energy radiated into the upper half-space and the totally dissipated energy. Plot $q_a$ as a function of the molecule's vertical position $z_o/\lambda$. Use the plot range of $z_o/\lambda = [0\,..\,2]$ and $q_a = [0\,..\,1]$.

**Problem 10.5** For a dipole sitting on an air-dielectric interface ($n_1 = 1$, $n_2 = 1.5$) calculate the ratio between the energy radiated into the upper half-space and the energy radiated into the lower half-space. Perform the calculations separately for a horizontal and a vertical dipole.

# References

[1] H. Metiu, "Surface enhanced spectroscopy," in *Progress in Surface Science* (I. Prigogine and S. A. Rice, eds.) **17**, 153–320, New York: Pergamon Press (1984).

[2] See, for example, L. Novotny, "Allowed and forbidden light in near-field optics," *J. Opt. Soc. Am. A* **14** 91–104 and 105–113 (1997), and references therein.

[3] L. M. Brekhovskikh and O. A. Godin, *Acoustics of Layered Media*. Berlin: Springer, first ed. (1990).

[4] A. Sommerfeld, "Über die Ausbreitung der Wellen in der drahtlosen Telegraphie," *Ann. d. Physik* **28**, 665–736 (1909).

[5] J. Zenneck, "Fortpflanzung ebener elektromagnetischer Wellen längs einer ebenen Leiterfläche," *Ann. d. Physik* **23**, 846–866 (1907).

[6] H. v. Hörschelmann, "Über die Wirkungsweise des geknickten Marconischen Senders in der drahtlosen Telegraphie," *Jb. drahtl. Telegr. u. Teleph.* **5**, 14–34 and 188–211 (1911).

[7] A. Sommerfeld, "Über die Ausbreitung der Wellen in der drahtlosen Telegraphie," *Ann. d. Physik* **81**, 1135–1153 (1926).

[8] H. Weyl, "Ausbreitung elektromagnetischer Wellen über einem ebenen Leiter," *Ann. d. Physik* **60**, 481–500 (1919).

[9] M. J. O. Strutt, "Strahlung von Antennen unter dem Einfluss der Erdbodeneigenschaften," *Ann. d. Physik* **1**, 721–772 (1929).

[10] B. V. der Pol and K. F. Niessen, "Über die Ausbreitung elektromagnetischer Wellen über einer ebenen Erde," *Ann. d. Physik* **6**, 273–294 (1930).

[11] G. S. Agarwal, "Quantum electrodynamics in the presence of dielectrics and conductors. I. Electrodynamic-field response functions and black-body fluctuations in finite geometries," Phys. Rev. A **11**, 230–242 (1975).

[12] A. Sommerfeld, *Partial Differential Equations in Physics*. New York: Academic Press, fifth ed. (1967).

[13] B. Hecht, D. W. Pohl, H. Heinzelmann, and L. Novotny, "'Tunnel' near-field optical microscopy: TNOM-2," in *Photons and Local Probes*, O. Marti and R. Möller, eds.,NATO Advanced Study Institute, Series E **300**, 93-107, Kluwer Academic Publishers, Dordrecht (1995).

[14] W. C. Chew, *Waves and Fields in Inhomogeneous Media*. New York: Van Nostrand Reinhold, first ed. (1990).

[15] W. Lukosz and R. E. Kunz, "Light emission by magnetic and electric dipoles close to a plane interface. I. total radiated power," *J. Opt. Soc. Am.* **67**, 1607–1615 (1977).

[16] I. Pockrand, A. Brillante, and D. Möbius, "Nonradiative decay of excited molecules near a metal surface," *Chem. Phys. Lett.* **69**, 499–504 (1994).

[17] J. K. Trautman and J. J. Macklin, "Time-resolved spectroscopy of single molecules using near-field and far-field optics," *Chem. Phys.* **205**, 221–229 (1996).

[18] R. X. Bian, R. C. Dunn, X. S. Xie, and P. T. Leung, "Single molecule emission characteristics in near-field microscopy," *Phys. Rev. Lett.* **75**, 4772–4775 (1995).

[19] L. Novotny, "Single molecule fluorescence in inhomogeneous environments," *Appl. Phys. Lett.* **69**, 3806–3808 (1996).

[20] H. Gersen, M. F. Garca-Parajo, L. Novotny, J. A. Veerman, L. Kuipers, and N. F. van Hulst , "Influencing the angular emission of a single molecule," *Phys. Rev. Lett.* **85**, 5312–5314 (2000).

[21] W. Lukosz and R. E. Kunz, "Light emission by magnetic and electric dipoles close to a plane dielectric interface. II. radiation patterns of perpendicular oriented dipoles," *J. Opt. Soc. Am.* **67**, 1615–1619 (1977).

[22] M. A. Lieb, J. M. Zavislan, and L. Novotny, "Single molecule orientations determined by direct emission pattern imaging," *J. Opt. Soc. Am. B* **??**, ??–?? (2004).